Preparation of Nanostructured Cellulose *via* Cr(III)- and Mn(II)-Transition Metal Salt Catalyzed Acid Hydrolysis Approach

You Wei Chen, Hwei Voon Lee,* and Sharifah Bee Abd Hamid

Nanostructured cellulose was successfully prepared from native cellulose using a homogeneous catalytic H_2SO_4 hydrolysis pathway in the presence of Cr(III)- and Mn(II)-transition metal salts as the co-catalyst. The effect of transition metal salts with different valence states (Cr^{3+} and Mn^{2+}) on the physicochemical properties (chemical characteristics, crystallinity index, nano-structure, thermal stability, and morphology) of prepared nanocellulose was investigated. Interestingly, TEM micrographs showed that the Cr(III)-treated and Mn(II)-treated nanocellulose exhibited a web-like nanostructured-surface with average diameters of 44.7 ± 13.2 nm and 58.4 ± 15.3 nm, respectively. XRD study revealed that the crystallinity of nanocellulose was increased because the catalytic degradation of the less crystalline regions of cellulose occurred at a faster rate than its crystalline phases. Cr(III)-treated nanocellulose was capable of rendering a higher crystallinity index (75.6 ± 0.1%) compared with Mn(II)-treated nanocellulose (72.3 ± 0.4%). Furthermore, a dynamic light scattering (DLS) study revealed that Cr(III)-treated nanocellulose showed a smaller distribution range (92% at 14 to 135 nm) compared with Mn(II)-treated nanocellulose (92% at 607 nm). A higher valence state for the Cr(III)-cation, with a trivalent state (+3), rendered a more effective hydrolysis reaction compared with the Mn(II)-cation, with a divalent state (+2), for preparing the nanocellulose.

Keywords: Nanocellulose; Valence state; Crystallite structure; Selective catalytic hydrolysis; Morphology study

Contact information: Nanotechnology & Catalysis Research Centre (NANOCAT), Institute of Postgraduate Studies, University of Malaya, 50603 Kuala Lumpur, Malaysia;
**Corresponding author: leehweivoon@um.edu.my*

INTRODUCTION

Cellulose is a linear homo-polysaccharide composed of *β*-D-glucopyranose units linked with β-(1→4)-glucosidic linkages in the chair configuration. It is considered a renewable, environmentally friendly, and biocompatible raw material for the production of biodegradable products (Maepa *et al*. 2014). Nanocellulose can be prepared from natural cellulose *via* various hydrolysis treatments. Because of its nano-scale dimensions, nanocellulose exhibits various outstanding and excellent physicochemical properties compared with typical cellulose material, such as large specific surface area, high porosity, high aspect ratio, excellent tensile strength and modulus, and biodegradability (Cao *et al*. 2015). Also, the source material generally has a low cost. For these reasons, many studies have been carried out on the synthesis of nanocellulose fibers as reinforcement agents in polymer nanocomposites (Zimmermann *et al*. 2010). Environmentally friendly polymer composite materials based on cellulose have great advantages for emerging industrial applications such as applications in the electronic, biomaterial, water treatment, pharmaceutical, magnetic, and medical fields (Kalia *et al*. 2011; Chirayil *et al*. 2014). Chirayil *et al*. (2014) mentioned that the addition of nanocomposites into thermoplastic

starch could enhance the tensile strength of the product significantly compared with pure isolated thermoplastic starch, and the addition of sugar beet chip nanofibrils isolated *via* high-pressure homogenization to a phenol formaldehyde and polyvinyl alcohol matrix demonstrated excellent reinforcement properties (Chirayil *et al*. 2014). Therefore, it is essential to isolate the nanocellulose from its micro-scale raw material with the purpose of maximizing the potential of the cellulose source to become the useful composite materials such as polyethylene oxide/cellulose nanocrystal (PEO/CNC) (Zhou *et al*. 2011) and poly(vinyl alcohol)/cellulose nanocrystal (PVA/CNC) (Huan *et al*. 2016).

Nanocellulose can be prepared from cellulosic materials *via* mechanical treatment, chemical treatment, or biological (enzymes) hydrolysis treatment (Fatah *et al*. 2014). Generally, a mechanical approach such as high-pressure homogenization, cryocrushing, ultrasonication, or grinding is the most direct method for the preparation of nanocellulose (Li *et al*. 2014b). However, the mechanical treatment pathway requires high energy consumption, repeated processing, or complex equipment (Lee *et al*. 2014). On the other hand, enzymatic hydrolysis is a costly treatment, the enzymes are difficult to recycle, and the treatment usually requires more time to complete the hydrolysis process (2 to 6 weeks) (Mora-Pale *et al*. 2011). In recent years, ionic liquids such as 1-butyl-3-methylimidazolium hydrogen sulfate ($BmimHSO_4$) have been proposed as a potential hydrolyzing catalyst for cellulose depolymerization process, and the results showed that high crystallinity nanocellulose (95.8%) was isolated successfully from cotton linter model compound (84.4%) via ionic liquid catalyzed hydrolysis process by using $BmimHSO_4$ at 90 ^{o}C for 1.5 h (Tan *et al.* 2015). In the same year, a new hydrolysis approach which comprised ethanol and peroxide solvothermal pretreatment followed by ultrasonic process has been developed by Li and his coworkers for isolation of nanocellulose (Li *et al.* 2016). They treated the wood flour with the proposed pretreatment under reaction conditions of 180 ^{o}C for 80 min, and the results revealed that the nanocellulose produced had higher crystallinity (79.37%) than raw material (70.72%) (Li *et al.* 2016). In spite of their prolific use, the capital cost for the nanocellulose production is one of the major concerns in the industrial applications. The utilization of ionic liquid is restricted for industrial scale applications due to most of the ionic liquids are expensive, incomplete chemical and toxicological data, and the process for recovery of the ionic liquid is a highly energy-consuming process (Wang *et al.* 2014). On the other hand, the application of ethanol and peroxide solvothermal hydrolysis approach for conversion of cellulose is always requires harsher conditions such as high temperature and longer pretreatment period (Li *et al.* 2016). Thus, from an economic viewpoint, this will eventually increase the capital cost of the production line and unfavorable for long term production in the industrial use.

For these reasons, strong acid hydrolysis by mineral acids such as sulfuric, phosphoric, and hydrochloric acid is a well-known method for the preparation of nanocellulose (Lee *et al*. 2014). The hydronium ions (H_3O^+) generated by mineral acid can effectively break down or hydrolyze the intramolecular and intermolecular bonding in cellulose fibers (Yahya *et al*. 2015). The depolymerization process of cellulose into its smaller dimensions normally happens faster on the defective crystalline parts in the long polymeric chains than the crystallinity phases as there are more active sites and defects regions for chemical reaction to be carried out (Usov *et al.* 2015). Although strong acid hydrolysis treatment is simple, some limitations still need to be considered, such as environmental pollution and difficulty in controlling the hydrolysis extent of cellulose, and the reaction is usually accompanied by uncontrollable over-degradation into undesired water-soluble monomers (*e.g.*, glucose), as well as the corrosion of the reactor vessel equipment (Hamid *et al*. 2015). To overcome this, dilute or organic acids have been proposed to create a milder reaction, but such treatment normally requires a higher reaction temperature (>150 °C) or longer hydrolysis time (>1 h) (Alvira *et al*. 2010), and it was

found to be less effective in reacting to the structure of lignocellulosic biomass (Yahya *et al*. 2015).

Recently, transition metal salt catalysts have received use as acid homogeneous catalysts for the cellulose hydrolysis process. Transition metal salt catalysts normally can be categorized based on their valence states, such as trivalent ($FeCl_3$, $Fe_2(SO_4)_3$, $CrCl_3$, $AlCl_3$) or divalent ($FeCl_2$, $FeSO_4$, $CuCl_2$), and have high potential for acting as the hydrolysis catalyst for the degradation of the glycosidic linkage of cellulose during acid hydrolysis treatment (Liu *et al*. 2009; Yi *et al*. 2013). However, the valence state of the transition metal ion plays a significant role in hydrolysis efficiency. Li *et al.* (2015) reported that the crystallinity of nanocellulose was improved by approximately 19% from native cellulose after being treated by a trivalent Fe(III)-metal ion catalyst (Li *et al*. 2015). However, Mazlita's study found that the divalent Ni(II)-inorganic salt with an optimum pH of 5.0 (1.0 M) was capable of increasing the crystallinity of the treated nanocellulose by approximately 7% compared with untreated cellulose (Yahya *et al*. 2015). The results of another study done by Li *et al.* (2013) to investigate the effect of Fe(III) and Cu(II) transition metal ions on the yield of nanocellulose indicated that nanocellulose treated with the ion with a higher oxidation state (Fe(III), which is trivalent) rendered an extra 7% higher crystallinity compared with a Cu(II)-catalyzed hydrolysis reaction (Li *et al*. 2013).

To achieve a technically feasible and high selectivity controllable hydrolysis pathway, $Cr(NO_3)_3$- and $Mn(NO_3)_2$ transition metal salts have been selected as a potential hydrolyzing agent for cellulose depolymerization process. Based on reported studies, Cr(III)- and Mn(II)-based transition metal catalysts have been found to have highly effective in breakage of extensive network of glycosidic linkage and hydrogen bonding within the cellulose matrix to separate cellulose fibrils. Shi *et al.* (2013) pointed out that, when the microcrystalline cellulose hydrolyzed by the [BMIM]Cl ionic liquid (9 mol%) in the presence of $MnCl_2$ (3 mol%) as co-catalyst, a maximum HMF yield of 66.5% (selectivity 74.43%) was obtained under the reaction conditions of 120 ^oC and 1 h (Shi *et al*. 2013). On the other hand, Peng *et al*. (2010) reported that $CrCl_3$ transition metal salt was highly effective for conversion of cellulose into its simpler form (*i.e.* levulinic acid) under the optimized conditions of 200 ^oC for 180 min, with the maximum yield of 67 mol%. During the catalytic hydrolysis, the metal salt catalyst acts as a Lewis acid that possessed of high hydrolyzing ability to depolymerize the cellulose by disrupting its bonding system, and thus the enhanced the fermentable sugar yield as compared with dilute acid hydrolyzing alone (Nguyen and Tucker 2002). Therefore, by combining a $Cr(NO_3)_3$ metal ion catalyst with dilute H_2SO_4, one can potentially overcome the drawback of dilute acid hydrolysis since the combination of both pretreatment may initiate a synergistic effect, thus enhancing the hydrolysis efficiency of cellulose depolymerization into nanostructured cellulose under controllable reaction conditions. In fact, the advantage of using transition metal salt (*e.g.* Mn(II)- and Cr(III)-) instead of strong H_2SO_4 for acid hydrolysis is reducing acid consumption for depolymerization process, which prevent corrosive issues, increase the selectivity of nanocellulose product with lower severity conditions (mild temperature and shorter hydrolysis period).

Previous studies have reported on the utilization of different isolation methods for the production of cellulose nanoparticles. However, to the best of our knowledge, no studies considering on the isolation of solid intermediate crystallite nanocellulose *via* a Cr(III) and Mn(II)-catalyzed sulfuric acid hydrolysis process rather than water soluble reducing sugars. In addition, only limited studies have reported on the correlation effect between different valence states (+3, +2) transition metal salts and hydrolysis efficiency for producing nanocellulose with a higher crystallinity. In this context, the objectives of this study are as follows: (i) to explore the feasibility and the practicability of isolating nanocellulose from native cellulose *via* Cr(III)- and Mn(II)-catalyzed H_2SO_4 acid

hydrolysis; (ii) to investigate the correlation between transition metal salts with divalent (Mn^{2+}) and trivalent (Cr^{3+}) catalysts on the efficiency of catalytic hydrolysis during cellulose depolymerization process; and (iii) to examine the changes in the physicochemical properties during conversion from macro- to nanocellulose in terms of crystallinity (X-ray diffraction; XRD), particle size distribution (dynamic light scattering; DLS), morphology (field emission scanning electron microscopy; FESEM, transmission electron microscopy; TEM, and atomic force microscopy; AFM), and thermal stability (thermogravimetric analysis; TGA). This study will explore the feasibility of using a new hydrolysis route to produce cellulose nanoparticles *via* a transition metal-catalyzed sulfuric acid hydrolysis approach that has the advantages of simplicity in operation and that no complicated equipment is required.

EXERIMENTAL

Materials

Alpha cellulose (white powder, analytical grade) was purchased from Sigma-Aldrich (USA). The chemical reagents used in this study, such as sulfuric acid (H_2SO_4, 95% to 97% purity), manganese (II) nitrate [$Mn(NO_3)_2$], and chromium (III) nitrate [$Cr(NO_3)_3$], were obtained from R&M Chemicals (Malaysia). All chemicals were used in their received form without further purification processing.

Methods

Preparation of nanocellulose

One gram of cellulose was treated with a mixture of 4 wt.% sulfuric acid and 25 mM of $Mn(NO_3)_2$ or $Cr(NO_3)_3$ transition metal salt catalyst. The suspension was heated to 80 °C for 45 min to complete the catalytic hydrolysis reaction. Subsequently, each sample was washed with cold deionized water and centrifuged repeatedly, followed by dialysis against distilled water until the pH of final suspension was around 4. The collected products were subjected to a freeze-drying process to obtain a fine white powder for further physicochemical characterization studies. The yield of nanocellulose was determined gravimetrically by drying the precipitate after the centrifugation (8000 rpm, 10 min) of 10 g aliquot at 40 ^{o}C under vacuum (Kos *et al.* 2014).

Physicochemical characterization

The Fourier transform infrared (FTIR) spectra of samples were analyzed with an FTIR spectrometer (Bruker IFS66/s, Germany) with a resolution of 4 cm^{-1} for 64 scans in the range of 4000 to 400 cm^{-1}. The sample was mixed with KBr powder and compressed into a pellet with a ratio of 1:10 (w/w).

The crystalline structure of samples was analyzed using a wide-angle X-ray diffraction (WAXRD) powder diffractometer (PANalytical Empyrean, Netherlands) with a Cu-Kα radiation source. The X-ray diffractograms were recorded from 5° to 60° while operating at a power of 40 kV and a current of 40 mA. The crystallinity index (*CrI*) of the samples was calculated using Segal's equation (Segal *et al*. 1959), as shown in Eq. 1,

$$CrI\ (\%) = (I_{200}\text{-}I_{am}) / I_{200} \times 100 \quad (1)$$

where I_{200} and I_{am} refer to the intensity of the crystalline (2θ = 22.5°) and amorphous regions (2θ = 18.5°) of the samples, respectively.

The surface morphology of the samples was characterized using a field-emission scanning electron microscope (FESEM) (Hitachi SU8030, Japan). The analysis was performed at an accelerating voltage of 5 kV with the working distance of 4 mm and a

secondary electron (SE) detector. The sample was coated with a layer of platinum using an auto-fine coater (JEOL JFC-1600, Japan) before analysis to prevent overcharging.

The particle dimensions and structure of nanocellulose were observed using a transmission electron microscope (TEM; Tecnai G^2 F20 Series, FEI, USA), which was operated at an acceleration voltage of 200 kV. A diluted suspension (0.01 wt.%) of the sample was sonicated to disperse it and dropped on a copper grid. The average diameter of each nanocellulose fiber was estimated using Image-J software for 300 measurements.

Atomic force microscopy (AFM) imaging of the samples was visualized with a model Dimension 3100 scanning probe microscope (Brand Veeco, Russia). A drop of the sample suspension (0.001 wt.%) was placed on a silicon wafer surface and dried in a desiccator. When the excess liquid evaporated, the samples were observed in tapping mode at room temperature. The AFM measurements were determined with NanoScope Analysis software for 300 samples.

The thermal behavior of the sample was analyzed by a model Q500 brand TA (Australia) thermogravimetric analyzer (TGA). The sample was heated from room temperature to 600 °C at a constant heating rate of 10 °C/min under a nitrogen atmosphere.

The particle size distribution and zeta potential of the yielded nanocellulose was examined by dynamic light scattering (DLS) using a Zetasizer NanoZS Instrument (Malvern, model ZEN 3600, UK). The samples were diluted in water with a concentration of 0.1 wt.% and well-dispersed by sonication treatment before analysis was carried out. Triplicate tests were carried out and the average values were reported.

RESULTS AND DISCUSSION

Chemical Structure Analysis (FTIR Study)

FTIR spectroscopic analysis of the native cellulose and chemically treated nanocellulose samples is shown in Fig. 1. The presence of the main peak at 3400 cm^{-1} is attributed to the O-H stretching band, caused by the hydrogen bonded hydroxyl group vibrations of cellulose I (Yahya *et al*. 2015). In addition, the peak at 2900 cm^{-1} corresponds to the aliphatic saturated symmetric C-H stretching vibration in cellulose (Hamid *et al*. 2015). The absorption peaks observed at 1640 and 1375 cm^{-1} are caused by the O-H bending mode of absorbed water and C-H bending within the polysaccharide aromatic rings of cellulose, respectively (Tan *et al*. 2015). FTIR peaks at 1430 cm^{-1} (CH_2 scissoring motion in cellulose), 1161 cm^{-1} (C─C ring stretching band), 1110 cm^{-1} (C─O─C pyranose ring stretching vibration), and 898 cm^{-1} (β─glycosidic linkages of cellulose glucose ring) are indicated as the typical bonds of cellulose I (I_β) structure (Leung *et al*. 2011; Kumar *et al*. 2014).

As also illustrated in Fig. 1, similar FTIR patterns were found for Mn(II)- and Cr(III)-treated nanocellulose, which indicated that the chemical structures of nanocellulose were not altered after catalytic acid hydrolysis process, where the typical structure of the parent cellulose was being preserved (Chen *et al.* 2016a, b). As reported by Singha *et al.* (2011), when the metal ions absorbed on the yielded nanocellulose, the wavenumbers of the functional groups will be shifted (Singha *et al.* 2011). However, the wavenumber position of the isolated nanocellulose remained similar to native cellulose; this suggested that there is no any metal ion introduced to the surface of nanocellulose fiber. Furthermore, the absence of NO_3^- peak at the signal of 1384 cm^{-1} indicated that the transition metal salt was completely removed during the centrifugation washing and dialysis process (Yahya *et al*. 2015).

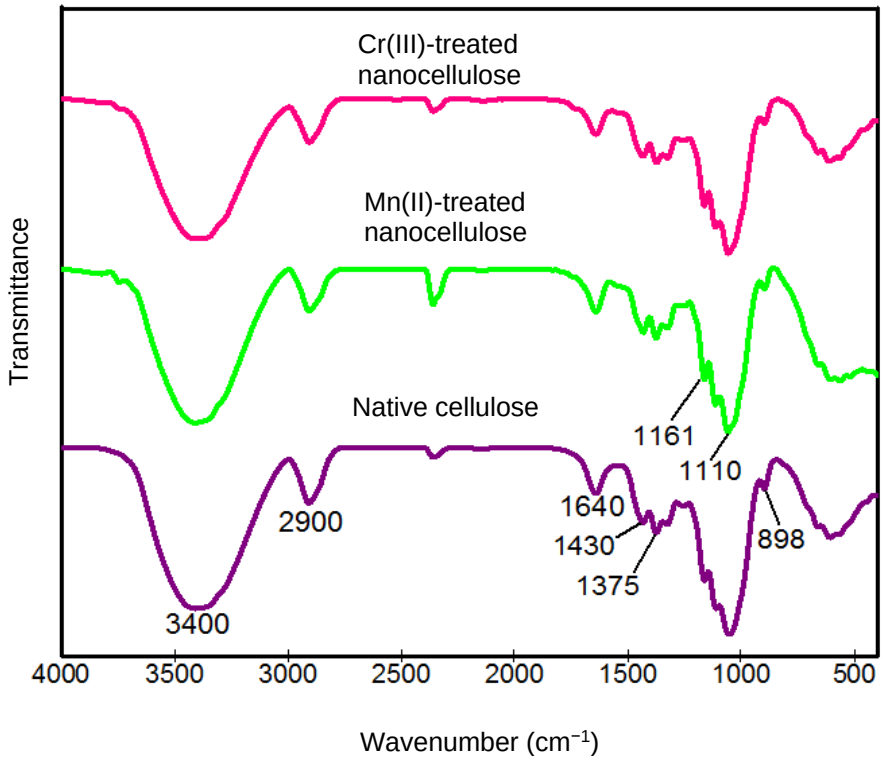

Fig. 1. FTIR spectra of native cellulose, Mn(II)-, and Cr(III)-treated nanocellulose

Crystal Structure Analysis (XRD Study)

Figure 2 shows the XRD diffraction patterns obtained for cellulose and nanocellulose. The crystallinity of cellulose in the isolated nanocellulose is the main factor affecting its mechanical strength in the polymer matrix (Chirayil *et al*. 2014). Nanocellulose showed similar diffraction patterns to those of native cellulose, with diffraction peaks at 2θ = 16.5°, 22.5°, and 34.6°, which can be accredited to the typical cellulose I structure (Yahya *et al*. 2015). This suggests that the crystal integrity in highly ordered crystallite regions of Mn(II)- and Cr(III)-treated nanocellulose remained unchanged after catalytic acid hydrolysis treatment. This finding is in agreement with the FTIR results. On the other hand, the peak intensity of nanocellulose at 2θ = 22.5° gradually increased compared with cellulose, which indicated the successive removal of soft less crystalline parts in cellulose fibers during hydrolysis treatment.

Using Segal's equation, the calculated crystallinity indices of cellulose, Mn(II)-treated, and Cr(III)-treated nanocellulose were found to be 43.7 ± 0.3%, 72.3 ± 0.4%, and 75.6 ± 0.1%, respectively. This showed a 58.9% and 70.7% increment for Cr(III)- and Mn(II)-treated nanocellulose compared with untreated cellulose, respectively. The results indicate that Cr(III)-metal ions rendered better hydrolytic efficiency and higher acid hydrolysis selectivity than Mn(II)-metal ions for breaking the glycosidic linkages of the cellulose defective crystalline regions while retaining crystalline regions in cellulose without over-hydrolysis to water-soluble monomer (*e.g.*, glucose) by-products. From the results, it can be clearly seen that Cr(III)-treated nanocellulose rendered the highest crystallinity, which enabled better mechanical properties and tensile strength; this is beneficial for composite material synthesis applications (Chen *et al*. 2011c; Tan *et al*. 2015; Yahya *et al*. 2015).

As for industrial applications, crystallinity of nanocellulose is the most important factor to be considered as it has a greater influence on reinforcing capabilities than aspect ratio (Silvério *et al.* 2013). In this study, the yielded nanocellulose prepared *via* transition metal ion catalyzed acid hydrolysis had higher crystallinity than that of nanomaterial

derived from various biomasses *via* different hydrolysis treatments. Son and his coworker (Son and Seo 2015) conducted a study by preparing the nanocellulose from three major cellulose sources (wood, non-wood and marine pulp) in nature via strong sulfuric acid hydrolysis, and the results revealed that all the yielded nanocellulose (*i.e.* softwood, hardwood; cotton linters, cattail; and red algae) exhibited lower crystallinity (ranged from 61.5 to 71.7%) as compared with our current study (72.3 to 75.6%). This finding suggests that concentrated acid hydrolysis has high tendency to attack the highly crystalline regions and is accompanied by over-degradation, such that most of the cellulose polymeric chains tended to be solubilized into water soluble reducing sugar (glucose). This eventually lowers the quality of nanocellulose.

A similar study has been reported by Hu *et al*. (2014) in which the authors had proposed two different isolation methods for nanocellulose production derived from borer powder, namely ammonium persulfate oxidative depolymerization and H_2SO_4 hydrolysis approach. The crystallinity index of both yielded nanocellulose samples isolated via these two hydrolysis treatments was 62.75 and 69.84%, respectively (Hu *et al.* 2014). The low crystallinity might be due to the harsh conditions applied during the course of treatment.

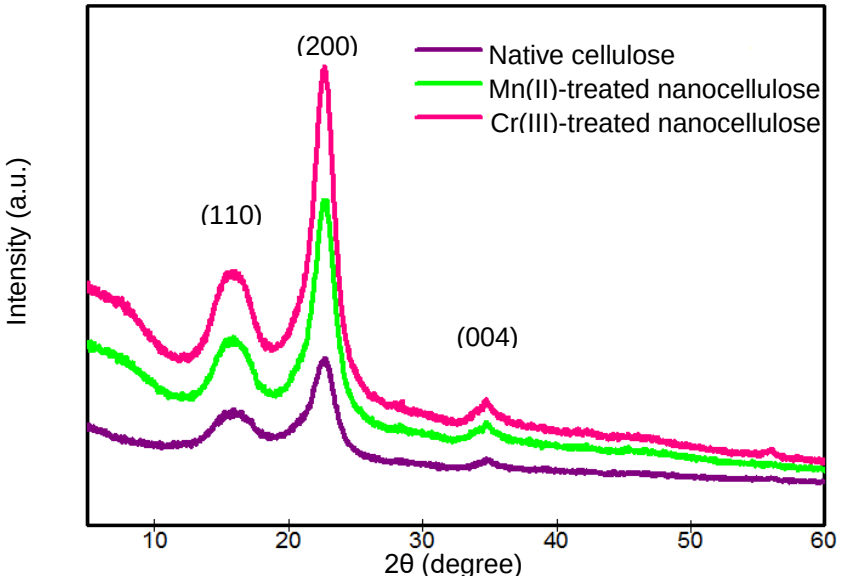

Fig. 2. XRD patterns of native cellulose, Mn(II)-, and Cr(III)-treated nanocellulose

On the other hand, in a practical manufacturing process, the yield of nanocellulose obtained after the hydrolysis treatment should also be taken into account in order to minimize the cost of large-scale commercial production with maximize the nanocellulose production. Therefore, a compromise should be made between the nanocellulose yield and its crystallinity in the maximum range. The percentage of yield of nanocellulose produced in this study ranged from 83.5 to 85%. This result is similar to those reported for palm tree cellulose (84%) (Hamid *et al.* 2014) and microcrystalline cellulose (86%) (Karim *et al.* 2014) hydrolyzed by $FeCl_3$ in HCl acidic medium but under higher temperature (91 to 98 ^oC) and longer hydrolysis duration (4 to 6 h) at optimum hydrolysis conditions. However, all the nanocellulose yields prepared via Cr(III)- and Mn(II)-catalyzed hydrolysis under mild reaction were much more higher than the value reported for the hydrolysis of cellulosic materials including rice straw cellulose (16.9%) (Jiang and Hsieh 2013), microcrystalline cellulose (28.6%) (Zhou 2012), and bamboo bleached fiber (30%) (Brito *et al.* 2012) via H_2SO_4 (~65 wt.%) hydrolysis procedure. A recent study (Tang *et al.* 2015) conducted by Tang's group found that the yield of nanocellulose produced via phosphoric acid hydrolysis followed by enzymatic hydrolysis was only able to achieve a yield of 23.98% with a crystallinity of 57.8%.

Table 1. Summary of Nanocellulose Characteristics Prepared using Transition Metal Salt Catalyzed Acid Hydrolysis Process

Cellulose Sample	Average hydrodynamic diameter [a] (nm)	Average diameter [b] (nm)	Crystallinity index [c] (CrI, %)	Yield [d] (%)
Untreated	> 1000	n/a	43.7 ± 0.3	n/a
Mn^{2+}-treated	693.2 ± 34.8	58.4 ± 15.3	72.3 ± 0.4	85.0 ± 0.5
Cr^{3+}-treated	281.6 ± 55.3	44.7 ±13.2	75.6 ± 0.1	83.5 ± 0.6

[a] Estimated from the dynamic light scattering (DLS) analysis
[b] Estimated from the transmission electron microscopy (TEM) analysis
[c] Crystallinity index estimated from Segal's method
[d] Reaction conditions: temperature, 80 °C; time, 45 min; concentration of H_2SO_4, 4 wt.%; concentration of metal salt catalyst, 25 mM

Surface Characterization Analysis (FE-SEM)

Scanning electron microscopy images of the cellulose and transition metal-treated nanocellulose are shown in Fig. 3. The cellulose material mostly consisted of aggregated long fibrils with an irregular shape (Fig. 3(a)). In addition, the compact structure of each cellulose fiber appeared to be assembled from hundreds to thousands of microfibrils, and each cellulose fiber was quite long and thus had a low aspect ratio (Tan *et al*. 2015). For Mn(II)- and Cr(III)-treated nanocellulose (Fig. 3(b) and (c)), it can be clearly observed that the original cellulose fibers were broken down and degraded to a great extent after hydrolysis treatment, which led to the long ribbon-like quality of the original fiber turning into short, rod-like structures.

The micro-sized cellulose fibrils tended to separate from the fibers' bundles, which resulted in intermittent breakdown in its fibrillar structure with more individualized, smaller fragments. These findings are in excellent accordance with the reported literature (Qua *et al*. 2011). The yielded nanocellulose produced in this study showed a finer fibrillar structure and reduced fiber diameter compared with native cellulose (23.1 ± 11.5 μm). Furthermore, it was observed that the Cr(III)-treated nanocellulose (15.9 ± 6.2 μm) had a smaller diameter than Mn(II)-treated nanocellulose (19.0 ± 8.4 μm) because of the successive hydrolysis treatment catalyzed by Cr(III) metal ions in the degradation of defective crystalline regions due to the attacking of metal ion catalysts in this less crystalline regions and lead to the hydrolytic cleavage of the *β*-1,4-glycosidic linkages in cellulose polymeric chains.

In the present study, finer and shorter nano-dimensional fibrils were expected in the nanocellulose samples treated by different transition metal salt catalysts; however, this was not obvious from the FESEM micrographs, as shown in Fig. 3. This was accredited to the strong intermolecular hydrogen bonding within the cellulose chains. As a result, the cellulosic fibrils tended to be agglomerated during the lyophilizing process (Qua *et al.* 2011).

More insight into the particle size and morphology of the nanocellulose fibers in suspension was obtained through transmission electron microscopy (TEM) and atomic force microscopy (AFM) analyses.

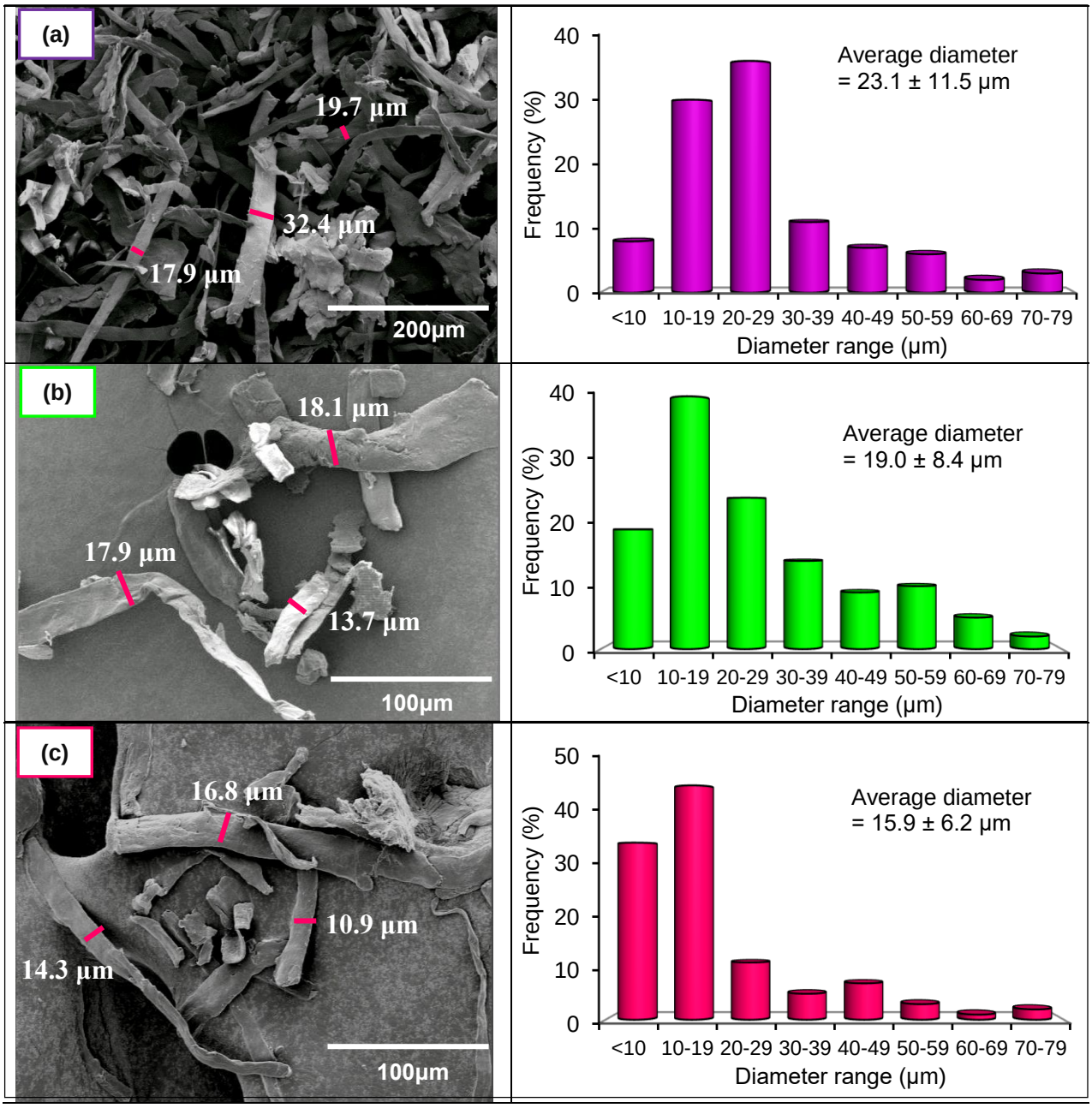

Fig. 3. FE-SEM images of (a) native cellulose, (b) Mn(II)-, and (c) Cr(III)-treated sample

Particle Size Analysis (DLS) and Zeta Potential Analysis

Dynamic light scattering (DLS) is one of the most suitable techniques for a rapid evaluation and preliminary screening of yielded nanocellulose particle size distribution as compared with the more established electron microscopic study (Kos *et al.* 2014). The DLS technique is not able to accurately measure for rod-like materials; however, quantitative results regarding the hydrodynamic diameter of nanoparticles could be obtained quickly.

Because the DLS method offers the advantages of fast and simple preparation process, the initial and rough analysis for determining the nanocellulose particle size in suspension still has been conducted by this method in many published studies (Yu *et al.* 2013; Li *et al.* 2015). Figure 4 shows the comparative particle size distributions for nanocellulose prepared by Mn(II)- and Cr(III)-catalyzed hydrolysis processes, estimated by dynamic light scattering (DLS) analysis in a water suspension (Fig. 4). Based on the results, the particle size distribution of Mn(II)-treated nanocellulose showed two main

groups: 91.6% were approximately 606.8 nm, and 8.4% were approximately 108.9 nm (Fig. 4(a)). Meanwhile, the hydrodynamic size distributions of the Cr(III)-treated nanocellulose, as shown in Fig. 4(b), were found to be 14.20, 135.8, and 458.5 nm with percentages of 2.2%, 89.7%, and 8.1%, respectively. Not surprisingly, the average hydrodynamic diameter of Cr(III)-treated nanocellulose (281.6 ± 55.3 nm) was found to be smaller than that of Mn(II)-treated nanocellulose (693.0 ± 34.8 nm), which indicated that Cr(III)-transition metal salt rendered better hydrolysis ability.

The colloidal performances of yielded nanocellulose were confirmed with zeta potential measurement. An absolute value lying within 0 to ± 15 mV reflects the onset flocculation and agglomeration of nanocellulose (Zhou 2012), whereas the values greater (or lower) than ± 25 mV were generally considered to be relatively stable for mutual repulsion to form a good stability colloidal suspension (Feng *et al.* 2015). In this study, the zeta potential for Mn(II)- and Cr(III)-treated nanocellulose was about ─42.5 and ─44.9 mV, respectively in the aqueous suspensions, thus indicative of the possibility to produce rather stable colloidal suspensions due to sufficient repulsive force. This is reasonably due to the presence of negatively charged sulfate groups introduced from H_2SO_4 into the nanocellulose surface during acid hydrolysis. This induced the increase in surface charges of the particles as well as led to the formation of an electrostatic layer covering the nanocellulose, thus minimizing it from aggregation and flocculation of particles (Hamid *et al.* 2015).

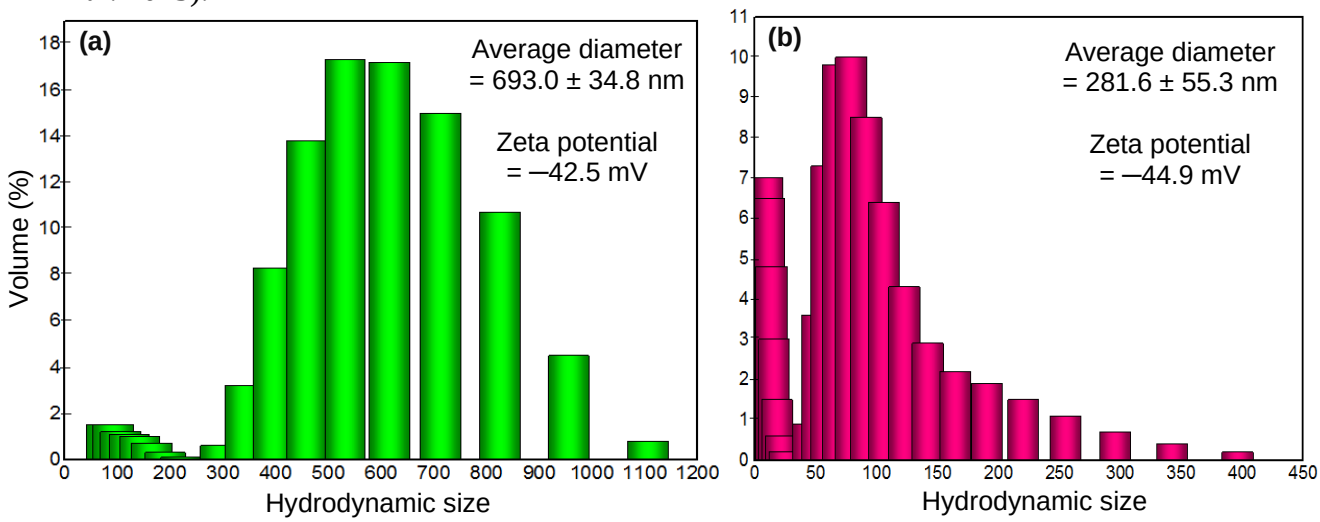

Fig. 4. Hydrodynamic size distributions of (a) Mn(II)- and (b) Cr(III)-treated nanocellulose

Morphological Analysis (TEM)

TEM images clearly illustrated that the nanocellulose isolated *via* both transition metal salt hydrolysis pathways exhibited entangled, complex spider-like network geometry with the presence of porous structures, as shown in Fig. 5. From the results, it was established that transition metal-catalyzed acid hydrolysis process was highly effective for hydrolyzing the micro-dimensional native cellulose fiber to its nanometer scale product. Based on the TEM micrographs, it was shown that nanocellulose treated with Mn(II)-metal ion catalyst had diameters mostly ranging between 40 and 80 nm, whereas Cr(III)-treated nanocellulose had a diameter range between 20 and 50 nm and were several microns long. The average fiber diameter showed that the former demonstrated a larger value (58.4 ± 15.3 nm) than the latter (44.7 ± 13.2 nm), with a fiber length of several micrometers. The smaller diameter of nanocellulose indicated that Cr(III) metal salt catalyst contributed to a highly efficient depolymerization process by attacking the defective crystalline parts at a faster rate than the crystallinity phases, as there are more active sites for chemical reactions to happen.

Additionally, some agglomeration of nanocellulose fibrils can be observed in certain places, while the rest are well separated. Similar phenomena were also reported from the preparation of cellulose nanofibrils from *Helicters isora* by acid hydrolysis (Chirayil *et al*. 2014). On the other hand, the entanglement structure among the yielded nanocellulose play an important role in force transferring from either fibrils to fibrils or matrix to fibrils to form a strong reinforcement when blended with other polymer materials (Tian *et al*. 2016).

In this study, the size distribution of all two types of nanocellulose (20 to 80 nm) was thus rather similar and relatively close to that reported for waste sackcloth (20 to 50 nm; Cao *et al*. 2015), borer powder (20 to 70 nm; Hu *et al*. 2014), rubberwood (10 to 90 nm; Jonoobi *et al*. 2011), sugarcane bagasse (20 to 60 nm; Kumar *et al*. 2014), flax (2 to 50 nm; Qua *et al*. 2011), and old corrugated container (15 to 80 nm; Zhang *et al*. 2015).

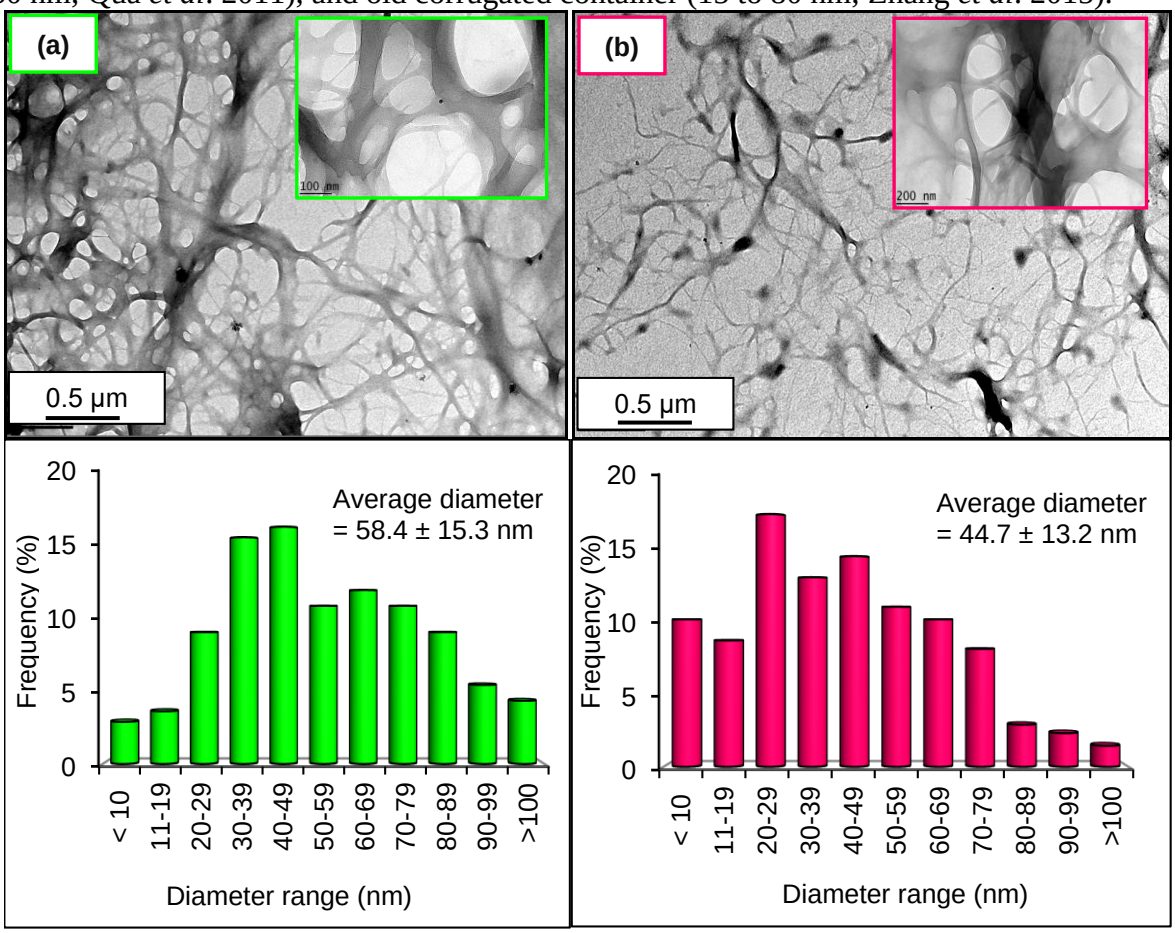

Fig. 5. TEM micrographs of (a) Mn(II)- and (b) Cr(III)-hydrolyzed nanocellulose

Morphological Study (AFM Analysis)

The surface morphology of yielded nanocellulose obtained using atomic force microscopy (AFM) analysis is displayed in Fig. 6. All the samples were observed in nano-dimensional rod-shape structure or needle-like nanoparticles. After the catalytic acid hydrolysis process, the original native cellulose long fibrils structure was successfully separated into smaller and finer fiber fragments (Lee *et al*. 2010). The AFM images show that the average diameters of Cr(III)-treated nanocellulose fibers (64.1 ± 31.7 nm) were smaller than those of Mn(II)-treated nanocellulose fibers (80.9 ± 30.3 nm). These findings correlate well with the TEM study.

The AFM results further verified that transition metal salt-catalyzed acid hydrolysis can easily break down the hydrogen bonding inside the cellulose matrix, mainly in

defective less crystalline parts, and leads to gradual disintegration of the micro-scale cellulose fibers into nano-sized cellulose.

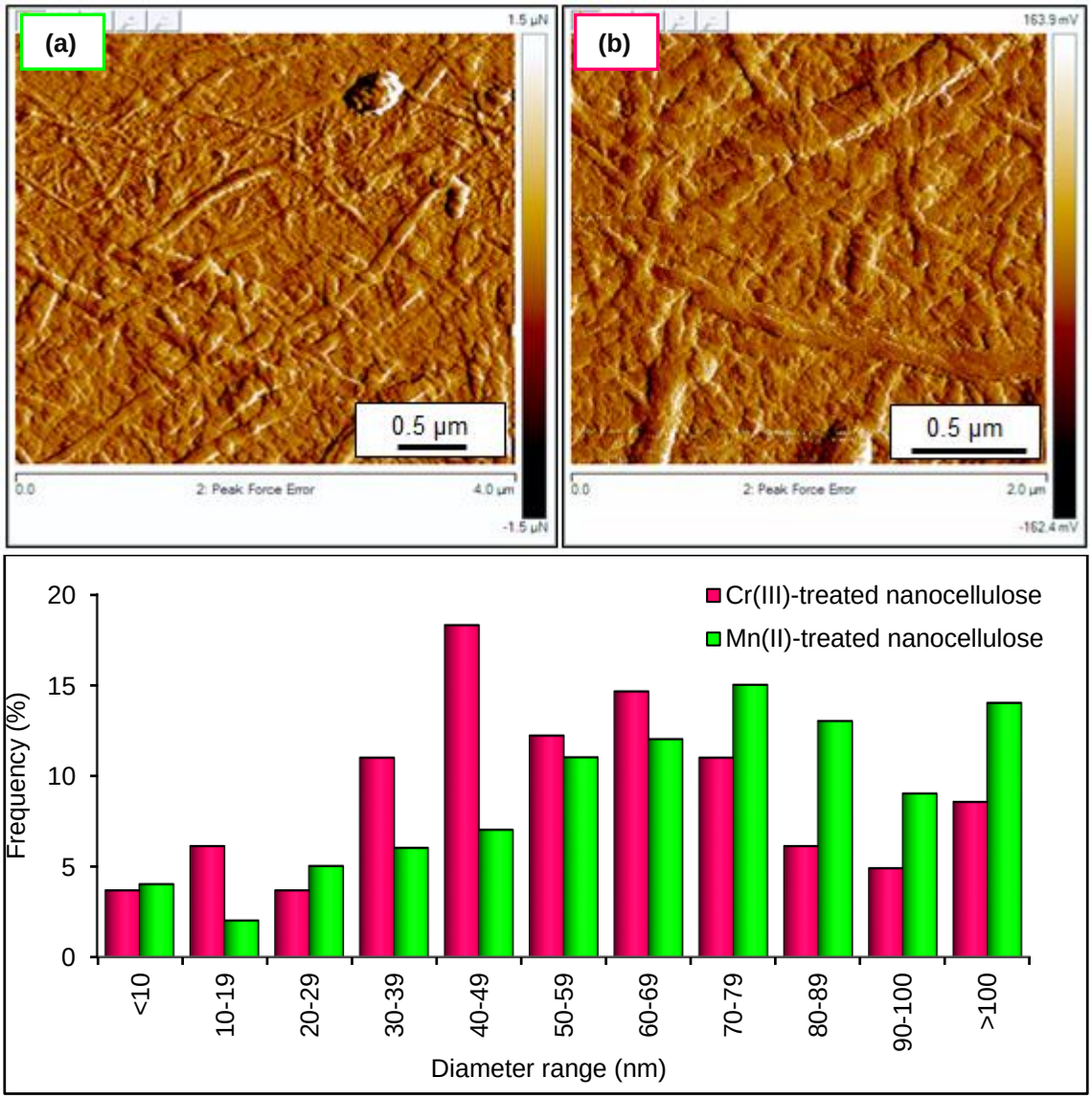

Fig. 6. AFM images and particle size distribution of (a) Mn(II)-, and (b) Cr(III)-treated nanocellulose

Thermal Stability Analysis (TGA Study)

Thermogravimetric (TG) curves and their derivatives (DTG) for cellulose and nanocellulose products are shown in Fig. 7. A minor weight loss that was found for all fiber samples below 100 °C can be attributed to the evaporation of absorbed moisture from the surroundings of the cellulose fiber. The native cellulose showed a typical decomposition behavior with an onset degradation temperature (T_{on}) of 250 °C and a maximum thermal degradation temperature (T_{max}) of 353.5 °C. The decomposition of the native cellulose showed only the one-step pyrolysis process, as shown in the DTG curve.

In the case of the produced nanocellulose, the degradation process occurred within a narrower range with lower T_{max} value (338 to 346 °C) compared with native cellulose, as summarized in Table 2. It was found that all the yielded cellulose nanoparticles possessed lower T_{max} values because of their smaller particle size, high specific surface area, and active sulfate groups (Cheng *et al*. 2014; Tan *et al*. 2015). A similar phenomenon was previously reported for the production of cellulose nanofibrils from sugarcane bagasse *via*

high-pressure homogenization because the produced nanomaterial consisted of a higher number of contact points to the heating source than crude cellulose (Saelee *et al*. 2016).

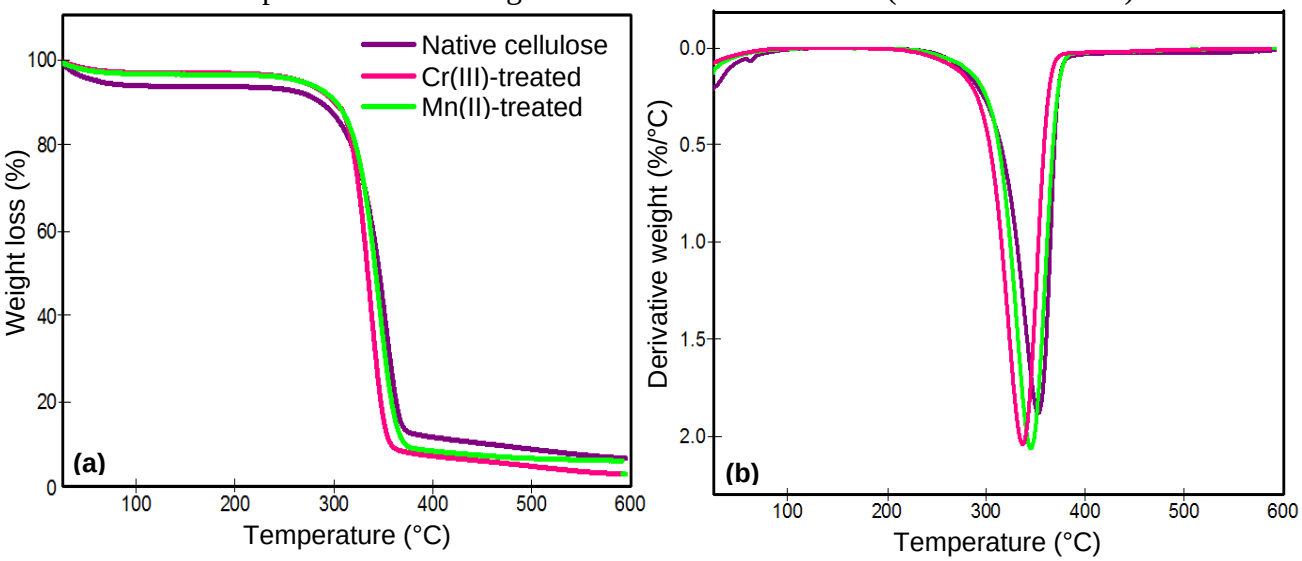

Fig. 7. (a) TG and (b) DTG curves of cellulose and yielded nanocellulose

In addition, the present finding was similar to several studies listed in Table 3, where the T_{max} value of yielded nanocellulose obtained from various biomass sources rendered lower values than that of crude cellulose material. The T_{max} values of yielded nanocellulose derived from wheat straw (T_{max} = 332.2 °C) (Chen *et al*. 2011), empty fruit bunch (T_{max} = 339 °C) (Jonoobi *et al*. 2011), and mulberry bark (T_{max} = 335 °C) (Li *et al*. 2009) are shown. Fortunately, all the cellulose nanoparticles were stable when the heating temperature was less than 280 °C. This is an important factor for the use of nanocellulose in various industrial applications, especially the thermoplastics field, as the processing temperature is normally higher than 200 °C (Cheng *et al*. 2014). Therefore, the thermal resistance of all the nanocellulose remained sufficient to ensure that nanocellulose can be processed at approximately 200 °C without any risk of degradation.

Table 2. TGA Profile of Nanocellulose Hydrolyzed by Cr(III)- and Mn(II)-Metal Salt

Sample	DTG: T_{max} (°C)
Native cellulose	353.5
Mn(II)-treated nanocellulose	346.0
Cr(III)-treated nanocellulose	338.0

Table 3. Thermal Properties of Nanocellulose Isolated from Different Biomasses

Starting material	T_{max} (°C)		Hydrolysis method	Reference
	Cellulose	Nanocellulose		
Wheat straw	337.5	332.2	Ultrasonic treatment	(Chen *et al*. 2011)
Empty fruit bunch	340	339	Chemo-mechanical	(Jonoobi *et al*. 2011)
Mulberry bark	397	335	H_2SO_4 hydrolysis	(Li *et al*. 2009)

Effect of Mn(II) and Cr(III) on Acid Hydrolysis Efficiency

Transition metal ions (Mn^{2+} or Cr^{3+}) showed a similar acid hydrolysis mechanism as inorganic acid (H_2SO_4) during the depolymerization of cellulose. The metal ions (Cr^{3+} and Mn^{2+}) were generated from transition metal salts capable of attaching to the high electronegativity of oxygen atoms in β-1,4-glycosidic bonds of the cellulose chain, which

resulted in weakening of the bond strength between pyranose rings in the amorphous region and thus led to the easy rupture of the cellulose chain into smaller fiber fragments (Li *et al*. 2014a). Compared with single-charge protons (+1) from typical mineral acids (*e.g.*, HCl or H_2SO_4), transition metal ions with higher valence states (*e.g.*, +2, +3) can efficiently hydrolytically cleave the extensive network in the cellulose fibers. This indicates that more protons are available to pair with more oxygen atoms to render an extensive reduction in particle size by breaking the glycosidic linkages in the cellulose structure (Zhao *et al*. 2011). In nature, the depolymerization process occurred in a faster rate on the defects structure in cellulose matrix as there is randomly ordered and more active sites for chemical degradation process to happen.

Generally, the efficiency of cellulose hydrolysis depends on the acidity of the hydrolysis catalyst. The acidity of the Mn(II)- and Cr(III)-metal ions is attributed to the deprotonation of metal-ligand complex ions. When the water molecules (H_2O) are bonded with the metal ions, they become more acidic than the metal ion alone (Li *et al*. 2013). This results in the generation of a higher concentration of H_3O^+ ion, as shown in Eqs. 2 and 3. Furthermore, a higher concentration of H_3O^+ ions was generated in the presence of Cr(III) ions as compared with Mn(II) ions because of its high valence state. Therefore, the Cr(III)-solution exhibits high acidity, which provides better acid hydrolysis efficiency for cellulose depolymerization (Zhao *et al*. 2007).

$$[Cr(H_2O)_6]^{3+} + 3H_2O \rightarrow [Cr(H_2O)_3(OH)_3] + 3H_3O^+ \quad (2)$$

[

$$Mn(H_2O)_6]^{2+} + 2H_2O \rightarrow [Mn(H_2O)_4(OH)_2] + 2H_3O^+ \quad (3)$$

CONCLUSIONS

1. Nanocellulose was successfully prepared by Mn(II)- and Cr(III)-catalyzed acid hydrolysis under a moderate temperature of 80 °C with a short preparation time (45 min). The removal of amorphous regions from the cellulose fibers was confirmed by XRD, FESEM, TEM, DLS, AFM, and TGA techniques.

2. Based on the results, the trivalent Cr^{3+} metal ion showed better hydrolysis and produced nanocellulose with a higher crystallinity (75.6 ± 0.1%) with a smaller diameter (46.3 ± 15.5 nm) compared with the divalent Mn^{2+} ion, with a nanocellulose crystallinity of 72.3 ± 0.4% and a diameter of 62.3 ± 13.9 nm.

3. The morphology study revealed that Cr(III)- and Mn(II)-treated samples appeared in smaller fragments compared with long and aggregated cellulose fibers. Furthermore, the prepared nanocellulose exhibited a spider web-like geometry, which indicated that the amorphous region in the compact cellulose fibers was removed during the catalytic acid hydrolysis reaction.

ACKNOWLEDGEMENTS

The authors are grateful for the financial support of the Minister of Science, Technology and Innovation (MOSTI) e-Science Fund (SF002-2015) and the University of Malaya Postgraduate Research Grant Scheme PPP (PG063-2015A).

REFERENCES CITED

Alvira, P., Tomas-Pejo, E., Ballesteros, M., and Negro, M. J. (2010). "Pretreatment technologies for an efficient bioethanol production process based on enzymatic hydrolysis: A review," *Bioresource Technology* 101(13), 4851-61. DOI: 10.1016/j.biortech.2009.11.093

Brito, B. L., Pereira, F., Putaux, J.-L., and Jean, B. (2012). "Preparation, morphology and structure of cellulose nanocrystals from bamboo fibers," *Cellulose* 19(5), 1527-1536. DOI: 10.1007/s10570-012-9738-9

Cao, Y., Jiang, Y., Song, Y., Cao, S., Miao, M., Feng, X., Fang, J., and Shi, L. (2015). "Combined bleaching and hydrolysis for isolation of cellulose nanofibrils from waste sackcloth," *Carbohydrate Polymers* 131, 152-158. DOI: 10.1016/j.carbpol.2015.05.063

Chen, W., Yu, H., Liu, Y., Hai, Y., Zhang, M., and Chen, P. (2011). "Isolation and characterization of cellulose nanofibers from four plant cellulose fibers using a chemical-ultrasonic process," *Cellulose* 18(2), 433-442. DOI: 10.1007/s10570-011-9497-z

Chen, Y. W., Lee, H. V., and Abd Hamid, S. B. (2016a). "Preparation and characterization of cellulose crystallites via Fe (III)-, Co (II)-and Ni (II)-assisted dilute sulfuric acid catalyzed hydrolysis process," *Journal of Nano Research* 41. DOI: 10.4028/www.scientific.net/JNanoR.41.96

Chen, Y. W., Lee, H. V., and Hamid, S. B. A. (2016b). "A response surface methodology study: Effects of trivalent Cr^{3+} metal ion-catalyzed hydrolysis on nanocellulose crystallinity and yield," *BioResources* 11(2), 4645-4662. DOI: 10.15376/biores.11.2.4645-4662

Chen, Y. W., Lee, H. V., Juan, J. C., and Phang, S. M. (2016c). "Production of new cellulose nanomaterial from red algae marine biomass *Gelidium elegens*," *Carbohydrate Polymers* 151, 1210-1219. DOI: 10.1016/j.carbpol.2016.06.083

Cheng, M., Qin, Z., Liu, Y., Qin, Y., Li, T., Chen, L., and Zhu, M. (2014). "Efficient extraction of carboxylated spherical cellulose nanocrystals with narrow distribution through hydrolysis of lyocell fibers by using ammonium persulfate as an oxidant," *Journal of Materials Chemistry A* 2(1), 251-258. DOI: 10.1039/C3TA13653A

Chirayil, C. J., Joy, J., Mathew, L., Mozetic, M., Koetz, J., and Thomas, S. (2014). "Isolation and characterization of cellulose nanofibrils from *Helicteres isora* plant," *Industrial Crops and Products* 59, 27-34. DOI: 10.1016/j.indcrop.2014.04.020

Fatah, I. Y. A., Khalil, H., Hossain, M. S., Aziz, A. A., Davoudpour, Y., Dungani, R., and Bhat, A. (2014). "Exploration of a chemo-mechanical technique for the isolation of nanofibrillated cellulosic fiber from oil palm empty fruit bunch as a reinforcing agent in composites materials," *Polymers* 6(10), 2611-2624. DOI: 10.3390/polym6102611

Feng, X., Meng, X., Zhao, J., Miao, M., Shi, L., Zhang, S., and Fang, J. (2015). "Extraction and preparation of cellulose nanocrystals from dealginate kelp residue: structures and morphological characterization," *Cellulose* 22(3), 1763-1772. DOI: 10.1007/s10570-015-0617-z

Hamid, S. B. A., Chowdhury, Z. Z., and Karim, M. Z. (2014). "Catalytic extraction of microcrystalline cellulose (MCC) from *Elaeis guineensis* using central composite design (CCD)," *BioResources* 9(4), 7403-7426. DOI: 10.15376/biores.9.4.7403-7426

Hamid, S. B. A., Zain, S. K., Das, R., and Centi, G. (2015). "Synergic effect of tungstophosphoric acid and sonication for rapid synthesis of crystalline nanocellulose," *Carbohydrate Polymers* 138, 349-355. DOI: 10.1016/j.carbpol.2015.10.023

Hu, Y., Tang, L., Lu, Q., Wang, S., Chen, X., and Huang, B. (2014). "Preparation of cellulose nanocrystals and carboxylated cellulose nanocrystals from borer powder of bamboo," *Cellulose* 21(3), 1611-1618. DOI: 10.1007/s10570-014-0236-0

Huan, S., Bai, L., Cheng, W., and Han, G. (2016). "Manufacture of electrospun all-aqueous poly(vinyl alcohol)/cellulose nanocrystal composite nanofibrous mats with enhanced properties through controlling fibers arrangement and microstructure," *Polymer* 92, 25-35. DOI: 10.1016/j.polymer.2016.03.082

Jiang, F., and Hsieh, Y.-L. (2013). "Chemically and mechanically isolated nanocellulose and their self-assembled structures," *Carbohydrate Polymers* 95(1), 32-40. DOI: 10.1016/j.carbpol.2013.02.022

Jonoobi, M., Khazaeian, A., Tahir, P., Azry, S., and Oksman, K. (2011). "Characteristics of cellulose nanofibers isolated from rubberwood and empty fruit bunches of oil palm using chemo-mechanical process," *Cellulose* 18(4), 1085-1095. DOI: 10.1007/s10570-011-9546-7

Kalia, S., Dufresne, A., Cherian, B. M., Kaith, B., Avérous, L., Njuguna, J., and Nassiopoulos, E. (2011). "Cellulose-based bio-and nanocomposites: A review," *International Journal of Polymer Science* 2011, 837875. DOI: 10.1155/2011/837875

Karim, M. Z., Chowdhury, Z. Z., Hamid, S. B. A., and Ali, M. E. (2014). "Statistical optimization for acid hydrolysis of microcrystalline cellulose and its physiochemical characterization by using metal ion catalyst," *Materials* 7(10), 6982-6999. DOI: 10.3390/ma7106982

Kos, T., Anžlovar, A., Kunaver, M., Huskić, M., and Žagar, E. (2014). "Fast preparation of nanocrystalline cellulose by microwave-assisted hydrolysis," *Cellulose* 21(4), 2579-2585. DOI: 10.1007/s10570-014-0315-2

Kumar, A., Negi, Y. S., Choudhary, V., and Bhardwaj, N. K. (2014). "Characterization of cellulose nanocrystals produced by acid-hydrolysis from sugarcane bagasse as agro-waste," *Journal of Materials Physics and Chemistry* 2(1), 1-8. DOI: 10.1007/978-3-642-27758-0_1162-2

Lee, H. V., Hamid, S. B. A., and Zain, S. K. (2014). "Conversion of lignocellulosic biomass to nanocellulose: Structure and chemical process," *The Scientific World Journal* 2014, 631013. DOI: 10.1155/2014/631013

Lee, J. M., Pawlak, J. J., and Heitmann, J. A. (2010). "Longitudinal and concurrent dimensional changes of cellulose aggregate fibrils during sorption stages," *Materials Characterization* 61(5), 507-517. DOI: 10.1016/j.matchar.2010.02.007

Leung, A. C., Hrapovic, S., Lam, E., Liu, Y., Male, K. B., Mahmoud, K. A., and Luong, J. H. (2011). "Characteristics and properties of carboxylated cellulose nanocrystals prepared from a novel one-step procedure," *Small* 7(3), 302-305. DOI: 10.1002/smll.201001715

Li, B., Xu, W., Kronlund, D., Määttänen, A., Liu, J., Smått, J.-H., Peltonen, J., Willför, S., Mu, X., and Xu, C. (2015). "Cellulose nanocrystals prepared via formic acid hydrolysis followed by TEMPO-mediated oxidation," *Carbohydrate Polymers* 133, 605-612. DOI: 10.1016/j.carbpol.2015.07.033

Li, R., Fei, J., Cai, Y., Li, Y., Feng, J., and Yao, J. (2009). "Cellulose whiskers extracted from mulberry: A novel biomass production," *Carbohydrate Polymers* 76(1), 94-99. DOI: 10.1016/j.carbpol.2008.09.034

Li, J., Xiu, H., Zhang, M., Wang, H., Ren, Y., and Ji, Y. (2013). "Enhancement of cellulose acid hydrolysis selectivity using metal ion catalysts," *Current Organic Chemistry* 17(15), 1617-1623. DOI: 10.2174/13852728113179990071

Li, J., Zhang, X., Zhang, M., Xiu, H., and He, H. (2014a). "Optimization of selective acid hydrolysis of cellulose for microcrystalline cellulose using $FeCl_3$," *BioResources* 9(1), 1334-1345. DOI: 10.15376/biores.9.1.1334-1345

Li, Y., Liu, Y., Chen, W., Wang, Q., Liu, Y., Li, J., and Yu, H. (2016). "Facile extraction of cellulose nanocrystals from wood using ethanol and peroxide solvothermal pretreatment followed by ultrasonic nanofibrillation," *Green Chemistry* 18(4), 1010-1018. DOI: 10.1039/C5GC02576A

Li, Y., Zhu, H., Xu, M., Zhuang, Z., Xu, M., and Dai, H. (2014b). "High yield preparation method of thermally stable cellulose nanofibers," *BioResources* 9(2), 1986-1997. DOI: 10.15376/biores.9.2.1986-1997

Li, J., Zhang, X., Zhang, M., Xiu, H., and He, H. (2015). "Ultrasonic enhance acid hydrolysis selectivity of cellulose with HCl-$FeCl_3$ as catalyst," *Carbohydrate Polymers* 117, 917-922. DOI: 10.1016/j.carbpol.2014.10.028

Liu, L., Sun, J., Cai, C., Wang, S., Pei, H., and Zhang, J. (2009). "Corn stover pretreatment by inorganic salts and its effects on hemicellulose and cellulose degradation," *Bioresource Technology* 100(23), 5865-5871. DOI: 10.1016/j.biortech.2009.06.048

Maepa, C. E., Jayaramudu, J., Okonkwo, J. O., Ray, S. S., Sadiku, E. R., and Ramontja, J. (2014). "Extraction and characterization of natural cellulose fibers from maize tassel," *International Journal of Polymer Analysis and Characterization* 20(2), 99-109. DOI: 10.1080/1023666X.2014.961118

Mora-Pale, M., Meli, L., Doherty, T. V., Linhardt, R. J., and Dordick, J. S. (2011). "Room temperature ionic liquids as emerging solvents for the pretreatment of lignocellulosic biomass," *Biotechnology and Bioengineering* 108(6), 1229-1245. DOI: 10.1002/bit.23108

Nguyen, Q. A., and Tucker, M. P. (2002). "Dilute acid/metal salt hydrolysis of lignocellulosics." Midwest Research Institute.

Peng, L., Lin, L., Zhang, J., Zhuang, J., Zhang, B., and Gong, Y. (2010). "Catalytic conversion of cellulose to levulinic acid by metal chlorides," *Molecules* 15(8), 5258-5272. DOI: 10.3390/molecules15085258

Qua, E. H., Hornsby, P. R., Sharma, H. S. S., and Lyons, G. (2011). "Preparation and characterisation of cellulose nanofibres," *Journal of Materials Science* 46(18), 6029-6045. DOI: 10.1179/1743289810Y.0000000019

Saelee, K., Yingkamhaeng, N., Nimchua, T., and Sukyai, P. (2016). "An environmentally friendly xylanase-assisted pretreatment for cellulose nanofibrils isolation from sugarcane bagasse by high-pressure homogenization," *Industrial Crops and Products* 82, 149-160. DOI: 10.1016/j.indcrop.2015.11.064

Segal, L., Creely, J., Martin, A., and Conrad, C. (1959). "An empirical method for estimating the degree of crystallinity of native cellulose using the X-ray diffractometer," *Textile Research Journal* 29(10), 786-794. DOI: 10.1177/004051755902901003

Shi, J., Gao, H., Xia, Y., Li, W., Wang, H., and Zheng, C. (2013). "Efficient process for the direct transformation of cellulose and carbohydrates to 5-(hydroxymenthyl) furfural with dual-core sulfonic acid ionic liquids and co-catalysts," *Rsc Advances* 3(21), 7782-7790. DOI: 10.1039/C3RA41062E

Silvério, H. A., Neto, W. P. F., Dantas, N. O., and Pasquini, D. (2013). "Extraction and characterization of cellulose nanocrystals from corncob for application as reinforcing agent in nanocomposites," *Industrial Crops and Products* 44, 427-436. DOI: 10.1016/j.indcrop.2012.10.014

Singha, B., Naiya, T. K., kumar Bhattacharya, A., and Das, S. K. (2011). "Cr(VI) ions removal from aqueous solutions using natural adsorbents–FTIR studies," *Journal of Environmental Protection* 2(06), 729-735. DOI: 10.4236/jep.2011.26084

Son, H. N., and Seo, Y. B. (2015). "Physical and bio-composite properties of nanocrystalline cellulose from wood, cotton linters, cattail, and red algae," *Cellulose* 22(3), 1789-1798. DOI: 10.1007/s10570-015-0633-z

Tan, X. Y., Abd Hamid, S. B., and Lai, C. W. (2015). "Preparation of high crystallinity cellulose nanocrystals (CNCs) by ionic liquid solvolysis," *Biomass and Bioenergy* 81, 584-591. DOI: 10.1016/j.biombioe.2015.08.016

Tang, Y., Shen, X., Zhang, J., Guo, D., Kong, F., and Zhang, N. (2015). "Extraction of cellulose nano-crystals from old corrugated container fiber using phosphoric acid and enzymatic hydrolysis followed by sonication," *Carbohydrate Polymers* 125, 360-366. DOI: 10.1016/j.carbpol.2015.02.063

Tian, C., Yi, J., Wu, Y., Wu, Q., Qing, Y., and Wang, L. (2016). "Preparation of highly charged cellulose nanofibrils using high-pressure homogenization coupled with strong acid hydrolysis pretreatments," *Carbohydrate Polymers* 136, 485-492. DOI: 10.1016/j.carbpol.2015.09.055

Usov, I., Nyström, G., Adamcik, J., Handschin, S., Schütz, C., Fall, A., Bergström, L., and Mezzenga, R. (2015). "Understanding nanocellulose chirality and structure-properties relationship at the single fibril level," *Nature Communications* 6. DOI: 10.1038/ncomms8564

Wang, Y., Song, H., Peng, L., Zhang, Q., and Yao, S. (2014). "Recent developments in the catalytic conversion of cellulose," *Biotechnology & Biotechnological Equipment* 28(6), 981-988. DOI: 10.1002/cctc.201000302

Yahya, M. B., Lee, H. V., and Hamid, S. B. A. (2015). "Preparation of nanocellulose *via* transition metal salt-catalyzed hydrolysis pathway," *BioResources* 10(4), 7627-7639. DOI: 10.15376/biores.10.4.7627-7639

Yi, J., He, T., Jiang, Z., Li, J., and Hu, C. (2013). "$AlCl_3$ catalyzed conversion of hemicellulose in corn stover," *Chinese Journal of Catalysis* 34(11), 2146-2152. DOI: 10.1016/S1872-2067(12)60718-9

Yu, H., Qin, Z., Liang, B., Liu, N., Zhou, Z., and Chen, L. (2013). "Facile extraction of thermally stable cellulose nanocrystals with a high yield of 93% through hydrochloric acid hydrolysis under hydrothermal conditions," *Journal of Materials Chemistry A* 1(12), 3938-3944. DOI: 10.1039/C3TA01150J

Zhao, H., Holladay, J. E., Brown, H., and Zhang, Z. C. (2007). "Metal chlorides in ionic liquid solvents convert sugars to 5-hydroxymethylfurfural," *Science* 316(5831), 1597-1600. DOI: 10.1126/science.1141199

Zhao, J., Zhang, H., Zheng, R., Lin, Z., and Huang, H. (2011). "The enhancement of pretreatment and enzymatic hydrolysis of corn stover by $FeSO_4$ pretreatment," *Biochemical Engineering Journal* 56(3), 158-164. DOI: 10.1016/j.bej.2011.06.002

Zhou, C., Chu, R., Wu, R., and Wu, Q. (2011). "Electrospun polyethylene oxide/cellulose nanocrystal composite nanofibrous mats with homogeneous and heterogeneous microstructures," *Biomacromolecules* 12(7), 2617-2625. DOI: 10.1021/bm200401p

Zhou, Y. M. (2012). "Effect of nanocellulose isolation techniques on the formation of reinforced poly(vinyl alcohol) nanocomposite films," *Express Polymer Letters* 6(10), 794-804. DOI: 10.3144/expresspolymlett.2012.85

Zimmermann, T., Bordeanu, N., and Strub, E. (2010). "Properties of nanofibrillated cellulose from different raw materials and its reinforcement potential," *Carbohydrate Polymers* 79(4), 1086-1093. DOI: 10.1016/j.carbpol.2009.10.045

Article submitted: March 22, 2016; Peer review completed: May 29, 2016; Revised version received and accepted: June 27, 2016; Published: July 13, 2016.
DOI: 10.15376/biores.11.3.7224-7241